Soft Matter

Linear versus Branched: Flow of a Wormlike Micellar Fluid Past a Falling Sphere

Journal:	*Soft Matter*
Manuscript ID	SM-ART-02-2021-000281.R3
Article Type:	Paper
Date Submitted by the Author:	22-Mar-2021
Complete List of Authors:	Wu, Shijian; FAMU-FSU College of Engineering, Chemical and Biomedical Engineering Mohammadigoushki, Hadi; FAMU-FSU College of Engineering, Chemical and Biomedical Engineering

Linear versus Branched: Flow of a Wormlike Micellar Fluid Past a Falling Sphere

Shijian Wu and Hadi Mohammadigoushki*
Department of Chemical and Biomedical Engineering,
FAMU-FSU College of Engineering, Tallahassee, 32310, United States
(Dated: March 25, 2021)

We report experiments on flow of wormlike micellar solutions past a falling sphere. By increasing the salt-to-surfactant concentration ratio, and beyond a viscosity peak, wormlike micelles experience a transition from linear to branched microstructure. Two viscoelastic wormlike micelles with salt to surfactant concentrations on each side of the viscosity peak are considered. Our results indicate three significant differences in flows of branched and linear micelles. First, while the sphere drag correction factor rapidly decreases upon increasing Weissenberg number in linear micelles, it shows an apparent local maximum at $Wi \approx 3$ in branched micelles. Second, despite its high viscoelasticity, the time-averaged flow of branched micelles around the falling sphere exhibits a fore-and-aft symmetry, while a strong negative wake is observed in linear micelles at relatively weaker flows. Third, branched micelles exhibit a stronger flow-induced birefringence than linear micelles in an otherwise identical condition. Our hypothesis is that subject to strong flows around the falling sphere, branched micelles can relax much more efficiently than linear wormlike micelles through sliding of the branched junctions. This additional stress relaxation mechanism may facilitate micellar orientation, produce a marginal sphere drag reduction and a Newtonian-like flow profile around the falling sphere. Finally, unsteady flow is observed in both linear and branched micellar solutions beyond some critical thresholds of the extensional Weissenber number. Our results corroborate a recently proposed criterion for onset of instability in flow of wormlike micelles past a falling sphere, thereby, suggesting that micellar branching does not affect the mechanism of flow instability.

* Corresponding author; hadi.moham@eng.famu.fsu.edu

I. INTRODUCTION AND BACKGROUND

Surfactants are amphiphilic molecules that can self-assemble into various morphologies including spherical, rod-like, sponges or lamellar [1]. The morphology of the aggregates is dictated by the packing parameter p[2], which is defined as $p = v/l_c a_0$, where v is the volume of the hydrophobic chain, l_c is the maximum effective length of the hydrophobic chain, and a_0 is the effective area per molecule at the surfactant/water interface[2]. The most common micellar shape is spherical. However, beyond a critical micelle concentration, the addition of salt or a counterion to surfactant solution gives rise to a geometrical transition to un-entangled rod-like micelles that at sufficiently high concentrations grow in length, overlap, and gradually form entangled networks that exhibit strong viscoelastic properties. Interestingly, beyond a second critical salt to surfactant concentration ratio, some wormlike micelles show a maximum in their rheological properties (e.g. the zero-shear-rate viscosity or the relaxation time) [3–8]. The drop in the rheological properties has been related to yet another geometrical transition from linear to branched wormlike micelles[9]. It has been suggested that the branches in micelles can be thought of sliding connections that provide additional stress relaxation mechanism to micelles, thereby, giving rise to a low viscosity[10].

Wormlike micellar fluids have received wide-spread applications in an array of industrial operations including as viscosity modifiers in foodstuffs, paints, personal care products[11, 12]. In addition, entangled wormlike micellar fluids are widely used in oil-field operations during which they constantly interact with particles[13, 14]. Therefore, a fundamental understanding of the nature of interactions between particles and flow of wormlike micelles is critical for the optimal processing in industrial settings. However, understanding the nature of interactions between solid particles and wormlike micelles offers a considerable challenge. Hence, recent studies have mostly investigated the flow of wormlike micelles past a falling sphere as a first step towards a better understanding of the flow of wormlike micelles in porous medium with packed particles[15–19].

Entangled wormlike micellar fluids share many similarities with viscoelastic polymer solutions, however, unlike polymers, surfactants are weakly bound together by non-covalent bonds in wormlike micelles, and constantly undergo breakage and recombination[20]. The possibility of micellar breakage and reformation is believed to have given rise to an interesting instability in flows of wormlike micelles past a falling sphere[16, 17]. It has been shown that beyond a critical threshold, a sphere falling in wormlike micellar solutions may undergo an instability that is characterized by temporal fluctuations in sphere sedimentation velocity or the flow of wormlike micelles around the sphere[17]. This instability is believed to be tied to strong extensional flows in the wake of the falling sphere[17, 21], and caused by flow-induced micellar chain scission in the bulk scale [21]. Since the earliest work of Jayaraman and Belmonte[15], many research groups have investigated the effects of various parameters or conditions on this instability including, the effects of micelles relaxation spectrum[22], chemistry of the surfactant[23], sphere boundary conditions[19] and the micellar concentration[24]. More recently, Sasmal and co-workers have used the Vasquez-Cook-McKinley (VCM) model and reproduced this flow instability[25]. For a more detailed discussion, readers are referred to a recent review on complex flows of wormlike micelles (where a combination of shear and extension is relevant)[26].

Flow around a falling sphere is highly complex and non-viscometric. Near sphere and on its flanks, a strong shear flow exists, while farther away from the sphere, downstream of the sphere center of mass, the extensional flow is strong and dominant. It has been suggested that the flow instability associated with the falling sphere occurs in the wake of the sphere where extensional flows are dominant[16, 17]. Although flow instabilities in microfluidic bend device are not highly impacted by micellar branching[27], recent experimental studies have illustrated that the uni-axial extensional flow of wormlike micelles is strongly affected by the microstructure of the wormlike micelles [28–30]. In particular, Chellamuthu & Rothstein[28] studied the effects of micellar branching on extensional rheology of a wormlike micellar solution based on cetyltrimethylammonium bromide/sodium oleate (CTAB/NaOA) using a combination of capillary breakup extensional rheometery and filament stretching extensional rheometery. These researchers illustrated that as the micellar branches grow in this system, the dimensionless extensional viscosity (or Trouton ratio, Tr) decreases until it levels off around $Tr \approx 3$. The Trouton ratio is defined as the ratio of the apparent extensional viscosity to that of the zero-shear rate viscosity. According to Chellamuthu & Rothstein, highly branched micelles behave similarly to Newtonian fluids due to additional stress relaxation mechanism provided by sliding branched junctions. More recently, Sachsenheimer et al.[30] and Omidvar et al.[29] demonstrated that filament lifetime in uniaxial extensional flows of branched micelles scales differently with zero-shear rate viscosity η_0 than the linear wormlike micelles. The above studies suggest that sphere sedimentation dynamics in wormlike micelles, where extensional flows play a key role, should be strongly impacted by micellar branching.

Table (I) summarizes wormlike micellar systems that have been used in prior sphere sedimentation experiments. In summary, three micellar systems with different chemistries have been considered. While the two micellar solutions based on cetyltrimethylammonium bromide/sodium salicylate (CTAB/NaSal) and cetylpyridinium chloride/sodium salicylate (CPyCl/NaSal) are known to exhibit a viscosity peak beyond a critical salt to surfactant concentration ratio, the system of cetyltrimethylammonium p-toluenesulfonate/sodium chloride (CTAT/NaCl) is known to exhibit a plateau in zero-shear rate viscosity as the salt to surfactant concentration ratio increases[31].

Although the exact microstructures of these three model wormlike micelles have not

Solution	Conc. (mM/mM)	Critical Salt Conc. (mM)	Micelles Structure
CTAB/NaSal	9/9[15, 17]	11[32]	Linear
	25/25[17]	30[33]	Linear
	50/50[16]	45[33]	Lightly branched
CPyCl/NaSal	10/15[23]	9[34]	Branched
	25/18.75, 25/20.5[22]	21[22]	Linear
CTAT/NaCl	22/50[23]	–	Unknown
	42/100[18]	–	Unknown

TABLE I. List of micellar solutions used in prior sphere sedimentation experiments.

been directly evaluated via Transmission Electron Microscopy (TEM) imaging, one can predict formation of linear and branched micelles for salt concentrations below and above the critical concentration associated with the viscosity peak. Theoretical studies of Lequeux [35] have predicted that micellar branching should lower the viscosity, fundamentally supporting the transition from linear to branched micelles above the viscosity peak. Therefore, we have assessed the potential microstructure of wormlike micelles used in prior sphere sedimentation experiments based on their salt composition. Table (I) shows the concentration of salt in wormlike micellar solutions used for sphere sedimentation experiments along with the documented salt concentration associated with the viscosity peak in each system. It is clear that majority of the wormlike micellar systems used in previous studies consists of linear wormlike micelles. The only system that may be moderately branched is the CPyCl/NaSal system used by Zhang and Muller[23]. Note that in the latter study, the wormlike micelles differ both in their steady rheology (shear banding vs. non shear banding) as well as the surfactant chemistry. Additionally, the potential microstructure of CTAT/NaCl is not known because a viscosity peak is not typically observed in this system. Therefore, it is not possible to assess the effects of micellar branching in their studies.

To the best of our knowledge, a mechanistic understanding of the effects of micellar topology (linear vs. branched) on sphere sedimentation dynamics in wormlike micellar solutions is not available. In particular, it remains unclear how (if any) flow structure, fluid structure and/or drag correction factor are affected by micellar branching. Another open question is whether the flow instability caused by sphere motion is observed in branched micelles. According to Rothstein and co-workers, the stress relaxation mechanism due to sliding of branched points is highly effective such that it leads to a Newtonian-like Trouton ratio in uniaxial extensional flows[28]. Could this additional stress relaxation mechanism be more dominant than the flow-induced micellar breakage to delay or even eliminate this flow instability in branched micelles? Finally, in the case of flow instability in branched micelles, could the criterion proposed by Mohammadigoushki and Muller[17] be still valid? Mohammadigoushki and Muller performed a systematic study of sphere sedimentation in linear wormlike micellar solutions of CTAB/NaSal, and showed that a Weissenberg Number ($Wi = \lambda\dot{\gamma}$) defined by the shear rate is not suitable for explaining the threshold of instability. Instead, an extensional Weissenberg number($Wi_E = \lambda\dot{\varepsilon}_{max}$) provides a appropriate criterion to distinguish unsteady sphere motion from steady cases, where λ is the relaxation time of the wormlike micelles and $\dot{\varepsilon}_{max}$ is the maximum extensional rate in the wake of the falling sphere. The extensional rate is defined as $\dot{\varepsilon} = (\frac{\partial V_x}{\partial x})$, with V_x is the velocity of the fluid in the wake of a falling sphere along the direction of the sphere motion, and x is the position at the wake of a sphere.

The main objective of this paper is to investigate the effects of micellar microstructure (linear vs. branched) on dynamics of sphere sedimentation in wormlike micellar solutions. More specifically, we will investigate i) how micelles microstructure affects the flow of wormlike micellar solutions around the falling sphere, and ii) whether the previously developed criterion for the onset of instability can describe the onset of instability for different micellar microstructures. To accomplish this, we chose two sample wormlike micellar solutions based on CPyCl/NaSal at a fixed surfactant concentration but various salt to surfactant concentration ratios that correspond to each side of the viscosity peak. We used a combination of particle tracking velocimetry, particle image velocimetry and flow-induced birefringence

to evaluate the dynamics and orientation of linear and branched wormlike micellar chains around the falling sphere over a wide range of elasticity and inertia.

II. EXPERIMENTAL APPROACHES

A. Materials

Surfactant solutions are composed of CPyCl and NaSal in de-ionized water. Both CPyCl and NaSal were purchased from Sigma-Aldrich and used as received. The solutions were prepared by mixing a 25mM of CPyCl with various salt to surfactant concentration ratios in de-ionized water. The micellar solutions were mixed over a period of two days and equilibrated for four days before use. The salt to surfactant concentration ratio R was varied to determine the critical salt concentration associated with the maximum in the zero-shear rate viscosity or the relaxation time. Once the critical salt concentration is determined, one solution in each side of the maximum were selected to represent the linear and branched micellar solutions (see more details below). Additionally, various spheres with different densities (e.g., Nylon, Delrin, Teflon, Ceramic, Steel, Brass, Tungsten Carbide, and Aluminum) and diameters (a = 3/32″- 1/4″) were considered.

B. Rheological Measurements

Micellar solutions were characterized using both shear deformation and uni-axial extensional flows. The shear deformation experiments consist of linear and non-linear steady shear experiments that were performed in a commercially available rheometer (Anton-Paar MCR 302) using a Couette co-axial cylinders geometry with R_i = 13.35 mm and R_o = 14.53 mm. Here R_i and R_o denote the radii of the inner and the outer cylinders, respectively. Additionally, we characterized the extensional rheological properties of the wormlike micellar solutions via a dripping on a substrate capillary extensional rheometer (DoS) discussed in previous works[29, 36, 37]. The lower substrate in DoS experiments has a finite size to ensure that the fluid contact-line in pinned during filament thinning measurements[38].

C. Flow Visualizations

Flow visualization experiments were performed in a vertical cylindrical column with a height of $L = 1$ m and diameter $\Re = 85$ cm. The vertical glass cylindrical column is positioned inside a temperature controlled water bath made of acrylic. The water bath reduces the visual distortion by matching the refractive index of the glass tube cylinder and the wormlike micelles, which ensures a flat plane for particle image velocimetry (PIV) experiments. Further details on this setup are provided in our previous studies[22, 24]. Flow visualization experiments consist of particle tracking velocimetry (PTV), PIV and flow-induced birefringence (FIB). PTV was used to evaluate the velocity of the sphere center of mass[39], and the detailed form of flow structure around the falling sphere was characterized via the PIV technique[40]. For PIV related experiments, wormlike micelles were seeded with a small amount of tracing particles that does not affect the rheological properties of the fluids. Additional information

on the PIV setup is given in our prior publications[22, 24]. Finally, FIB was performed to evaluate the degree of micellar alignment and orientation around the falling sphere. When a linearly polarized light passes through a deformed micellar solution, an anisotropy in refraction index tensor is observed. Typically, in FIB experiments the important parameters are the retardation angle (δ) and the extinction angle (χ). The retardation angle is directly related to the optical anisotropy or the strength of the birefringence Δn as:

$$\delta = \frac{2\pi H \Delta n}{\Gamma}, \tag{1}$$

where Γ and H are the wave-length of the incident light and the optical depth of the birefringent sample. Two relevant orientations with respect to the flow direction may exist for wormlike micelles; the orientation of surfactant molecules that make up the wormlike micelles, and the orientation of the micelles themselves. The extinction angle quantifies the relative orientation of the wormlike micelles with respect to the flow direction. To obtain a full field FIB measurement, we have adopted the Osaki method[41]. Using this approach, the wormlike micellar fluids in the cylindrical column is placed between two crossed polarizers and a single wavelength incident light is used to illuminate the flow between two crossed polarizers. The wave-length of the light used in our FIB experiments $\Gamma \approx 680$ nm. The arrangement of the cross polarizers is changed as $0°/90°$ and $45°/135°$, and the light intensity is measured at different polarizers orientation. The light intensity at the $0°/90°$ orientation can be related to the birefringence as:

$$i_0 = \frac{2I^0}{I_0} = sin^2 2\chi sin^2(\frac{\delta}{2}), \tag{2}$$

where, I^0 and I_0 are the light intensity at orientation of 0 and the background light intensity in the absence of linear polarizers. The light intensity at the orientation angle of $45°$ is also given as:

$$i_{45} = \frac{2I^{45}}{I_0} = cos^2 2\chi sin^2(\frac{\delta}{2}). \tag{3}$$

By combining the above two equations, one can separately determine the retardation angle δ and the extinction angle χ as:

$$\delta = sin^{-1}(\sqrt{i_0 + i_{45}}), \qquad \chi = \frac{1}{2} tan^{-1}(\sqrt{i_0/i_{45}}). \tag{4}$$

Following FIB measurements at $0°/90°$ and $45°/135°$ orientation angles, compute i_0 and i_{45}, which are then used to determine the retardation and the extinction angle fields for the flow of wormlike micelles around the falling sphere.

III. RESULTS AND DISCUSSION

A. Rheological Measurements

First, we prepared a range of micellar solutions at a fixed surfactant concentration (25mM) and various salt to surfactant concentration ratios $R = 0.7 - 1$. The shear rheological properties of these solutions were characterized to determine the critical concentration associated

with the maximum in the zero shear-rate viscosity or the relaxation time. This critical concentration ratio occurs at $R = 0.84$. Therefore, we chose two solutions with $R = 0.8$ and $R = 0.92$ that correspond to either side of the viscosity peak curve (see the inset of Fig. 1(a)). TEM imaging of wormlike micelles is extremely challenging from sample preparation to the image acquisition stage with the equilibrium microstructure of the micelles often altered during sample preparation. Although the actual TEM images of these two wormlike micellar solution are not available, for a similar system (although at a different surfactant concentration; 100mM), Gaudino et al.[42] demonstrated a transition tructures above the critical concentration ratio. Moreover, for a similar solution with a surfactant concentration of 100mM, our diffusion based NMR spectroscopy measurements indicate that the transition around the viscosity peak is associated with the linear to branched micelles structures, respectively[43]. Therefore, based on the mechanical properties of these two solutions, and recent results of Gaudino et al.[42] and Holder et al. [43], we expect that wormlike micelles with $R = 0.8$ and $R = 0.92$ form linear and branched structures. Fig. 1 shows the rheological properties of these two wormlike micellar solutions measured at room temperature (T = 22 °C). Included in Fig. 1(a) are also the best fit to the Carreau-Yasuda model, which is given as:

$$\eta(\dot{\gamma}) = \eta_\infty + (\eta_0 - \eta_\infty)/[1 + (\dot{\gamma}/\dot{\gamma}^*)^\alpha]^{(1-n)/\alpha}. \quad (5)$$

In this model η_∞, $\dot{\gamma}^*$, α, and n denote the infinite shear rate viscosity, the shear rate for the onset of shear thinning, transient control factor and the shear thinning index, respectively. Fitting this model to the steady shear rheology data yields the above parameters which are listed in Table (II) below. Fig. 1(b) shows the Cole-Cole plot of these two micellar solutions along with the predictions of the single-model Maxwell model (continuous curve). The linear viscoelastic rheology of these two micellar solutions is best described by a single-mode Maxwell model within a wide range of frequencies (see also Fig. S1 in the supplementary materials). The inset of Fig. 1(b) shows the shear relaxation time of the micellar solutions with arrows pointing at the two solutions considered in this study. The relaxation times are obtained by fitting an m-mode Maxwell model to the linear viscoelastic rheology results with m varying for different salt to surfactant concentration ratios. For the two solutions considered in this study m = 1. Note that both zero-shear rate viscosity and the relaxation time of the linear micellar solution with $R = 0.8$ are higher than those measured for the branched micelles with $R = 0.92$. According to our rheological measurements, other linear wormlike micellar solutions with $R < 0.8$ are described by m-mode Maxwell models where m > 1. Based on our previous studies, sphere instability is not expected for linear wormlike micelles with a broad spectrum of relaxation times[22]. Additionally, the branched micellar solution is chosen as $R = 0.92$ to allow for a high density of branched junctions to form.

Besides shear rheology, the extensional rheological properties of these two micellar solutions were characterized with a DoS device (see Fig. 1(c,d)). Fig. 1(c) shows the mid-filament diameter as a function of time for these two micellar solutions and the best exponential fit to the elasto-capillary thinning regime denoted as solid lines. The mid-filament diameter in elasto-capillary regime varies as: $D = D_0 exp(-t/(3\lambda_E))$, where λ_E represent the extensional relaxation time of the viscoelastic solution. Additionally, the transient non-dimensional extensional viscosity (or the Trouton ratio) was calculated as a function of Hencky strain. The Trouton ratio is defined as $Tr = \eta_E/\eta_0 = -\sigma/(\eta_0 dD/dt)$, and the Hencky strain or the total accumulated strain is defined as: $\epsilon = 2Ln(D_0/D(t))$. The linear wormlike micellar fluid

shows a stronger strain hardening response than the branched system. The key rheological properties of these two micellar solutions are summarized in Table (II) below.

R = [NaSal]/[CPyCl]	η_0 [Pa.s]	η_∞ [Pa.s]	$\dot{\gamma}^*$	α	n	λ [s]	λ_E [s]	Tr_{max}
0.8	48	3×10^{-3}	0.04	3.8	0.01	23.2	6.1	300
0.92	24	7.3×10^{-2}	0.09	1.9	0.15	10.2	1.8	245

TABLE II. Rheological properties of the wormlike micellar solutions based on CPyCl/NaSal.

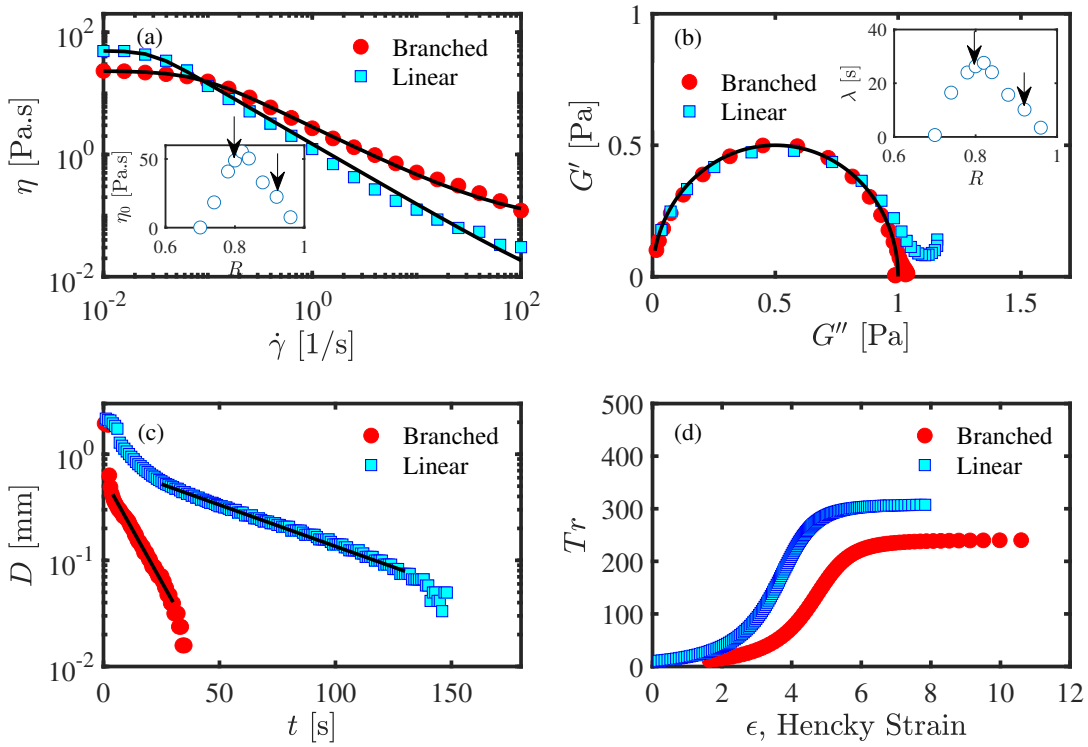

FIG. 1. (a) Steady shear viscosity as a function of imposed shear rate for the two micellar solutions. In this figure, the linear and branched micellar solutions are denoted by blue squares and red circles, respectively. Inset shows the zero-shear rate viscosity (η_0) at a fixed surfactant concentration and various salt to surfactant concentration ratios (R). Two arrows indicate the linear and the branched micellar solutions considered in this study. The black curves show the best fits to Carreau-Yasuda model. (b) Cole-Cole plots of the linear and branched micellar solutions. Inset shows the shear relaxation time (λ) of the micellar solution at a fixed surfactant concentration and various salt to surfacatant concentration (R). Two arrows indicate the linear and the branched micellar solutions considered in this study. The black curves are the best fitted single-mode Maxwell model. (c) mid-filament diameter (D) as a function of time for both the linear and branched wormlike micelle systems. The black curves indicate the best exponential fits to the elasto-capillary thinning regime. (d) Transient Trouton ratio Tr as a function of Hencky strain ϵ for linear and branched micellar solutions.

Subsequent to rheological characterizations, sphere sedimentation experiments were performed in these two micellar fluids. In the following we discuss the results by first explaining the results of drag correction factor on steady and unsteady sphere sedimentation regimes in linear vs. branched micelles. Then, we provide a more in-depth discussion about the detailed form of flow structure and the flow-induced birefringence around the falling sphere. Finally, we compare the unsteady flow structures around the falling spheres in linear and branched micelles and discuss the proposed criterion for the onset of flow instability.

B. Drag Correction Factor

In his seminal work George G. Stokes obtained the analytical solution for sphere sedimentation velocity in an un-bounded viscous fluid at vanishingly small Reynolds number as: $V_{Stokes} = 2(\rho_s - \rho_f)ga^2/9\eta_0$, where ρ_s, ρ_f and a represent the sphere density, the fluid density and the sphere diameter, respectively. In experiments with wormlike micellar solutions, the fluid is highly viscoelastic and spheres are no longer moving in an un-bounded domain. Therefore, in line with previous literature, we use a wall correction factor (or widely known as the drag correction factor) to evaluate the extent of drag reduction in sphere sedimentation experiments with wormlike micelles. The drag correction factor can be defined as: $K = V_{Stokes}/V_{max}$, where V_{max} is the measured sedimentation velocity of the sphere center of mass. Fig. 2 shows the drag correction factor as a function of Weissenberg number in the linear and branched wormlike micellar solutions. Weissenberg number is defined as $Wi = \lambda\dot{\gamma}$, where the characteristic shear rate is expressed as $\dot{\gamma} = V_{max}/a$. Note that the results of Fig. 2 are reported for various sphere to column size ratios $a/\Re = 0.018 - 0.074$, and each experiment has been repeated at least three times.

The empty symbols in Fig. 2 denote experiments with steady sphere motion while filled symbols represent unsteady sphere sedimentation cases. For unsteady sphere sedimentation cases, V_{max} is the time-averaged velocity of the sphere center of mass. Note that steady and unsteady sphere sedimentation behavior is observed both in the linear and branched micellar solutions. As expected, at low Wi numbers ($Wi < 1$), the drag correction factor for both linear and branched micelles are close to unity with K varying as $1.1 < K < 1.25$. As the flow around the falling sphere is strengthened (i.e. Wi increases) the wall correction factor drops for both linear and branched wormlike micelles. At $Wi > 1$, the drag correction factor in branched and linear micelles differ in two ways: First, the drag correction factors in branched micelles are larger than those measured for the linear micellar solution. Second, the drag correction factor in branched micellar system shows an apparent maximum approximately at $Wi \sim 3$ with a drag correction factor $K_{max} \approx 0.75$. In viscoelastic fluids, the drag correction factor is affected by the ratio of the sphere size to that of the boundary size (here $a/\Re$), the extent of shear thinning and elasticity (i.e., Normal stress differences, N_1) $K \sim f(a/\Re, \eta(\dot{\gamma})/\eta_0, N_1)$. Mena et al.[44] showed for an inelastic shear-thinning fluid the drag correction factor can be approximated as:

$$K = \frac{\eta(\dot{\gamma})/\eta_0}{1 - f(a/\Re)(\eta(\dot{\gamma})/\eta_0)}, \tag{6}$$

where Faxen's series $f(a/\Re)$ is given as: $f(a/\Re) = 2.1044(a/\Re) - 2.0888(a/\Re)^3 + 0.9481(a/\Re)^5$. Included in Fig. 2 are also the predictions of Mena et al.[44] for the two wormlike micellar

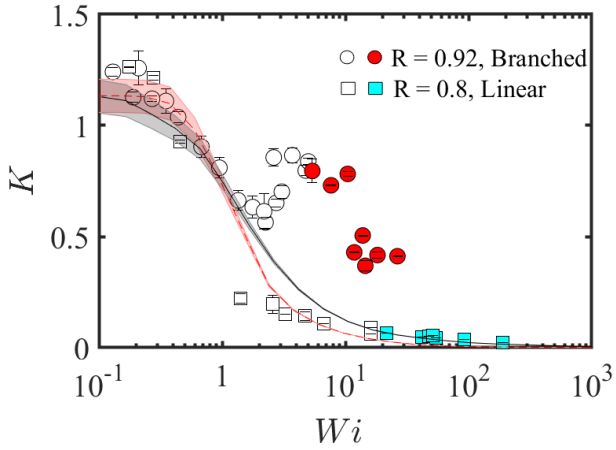

FIG. 2. drag correction factor K as a function of Weissenberg number, Wi for linear and branched micellar solutions. Empty and filled symbols denote the steady and unsteady sphere sedimentation behaviors. The red dashed-line and the continuous black line correspond to the predictions of Eq.(6) for linear and the branched micellar solutions, respectively.

solutions and various sphere to tube size ratios used in the experiments. The shaded area represents the extent to which the drag correction factor is affected by $a/\Re$ values used in this work. The deviations from Stokes' drag at low Wi numbers are due to the finite size of the spheres compared to the tube diameter. In general, Stokes' solution is valid for an infinite domain, whereas in these experiments the sphere to tube size ratio varies as $a/\Re = 0.018 - 0.074$. At this range of sphere to tube size ratio, sphere drag correction factors are affected by presence of the wall. At higher Wi numbers, the shear thinning effects become dominant and the drag reduction is reasonably independent of the sphere to tube size ratio. The two representative curves correspond to predictions of Eq. (6) for linear and branched micelles and deviations at high Wi numbers is caused by different degree of shear thinning in linear and branched micellar solutions (see shear thinning indices in Table (II)).

While the measured drag correction factors in linear wormlike micelles are in good agreement with the predictions of Mena et al. over the entire range of Wi numbers, significant deviations are reported in experiments with branched micelles for $Wi > 2$. We note that the maximum in drag correction factor is independent of the sphere to tube size ratio (see e.g., Fig. S2 in supplementary materials for a fixed $a/\Re$). Therefore, this apparent maximum in drag correction factor is presumably linked to presence of branched points in the solution with $R = 0.92$. Chen and Rothstein reported a similar, albeit modest, apparent maximum in their drag correction factor in a wormlike micellar solution based on CTAB/NaSal (50mM/50mM), which based on our estimate (see Table (I)) is lightly branched[16]. Therein, the maximum occurs right at the transition from steady to unsteady sphere sedimentation, which is reasonably consistent with our results.

C. Flow Profiles

To gain a more in-depth understanding of the nature of differences in drag correction factors in the branched and linear wormlike micelles, we turn our attention to the form of flow structure in steady flow experiments. Fig. 3 shows a series of time-averaged fluid velocity fields along the axis of the sphere center of mass for branched (Fig. 3(a)) and linear wormlike micelles (Fig. 3(b)) at various Wi numbers and fixed sphere to tube size ratios. Interestingly, flow of the branched micelles around the falling sphere exhibits a fore-and-aft symmetry even at the highest attainable Wi number for steady experiments (e.g., $Wi = 5$). The measured velocity profiles slightly deviate from Stokes' analytical solution, which has been reported elsewhere in Newtonian fluids[45]. Note that a similar fore-and-aft symmetry is reported in other experiments with different $a/\Re$ ratios (see e.g., Fig. S3 in the supplementary materials for $a/\Re = 0.056$). These results are rather surprising because in a strong viscoelastic branched wormlike micellar solution of $R = 0.92$, one anticipates a strong negative wake with a stagnation point flow to form downstream of the falling sphere. The stagnation point flow refers to a location downstream of the falling sphere center of mass where fluid velocity switches sign from positive (fluid moving in the direction of the sphere motion) to negative (fluid moving in the opposite direction of sphere motion). Interestingly, the Newtonian-like velocity profiles around the falling sphere in branched micelles are consistent with a drag correction factor around unity presented in Fig. 2.

On the other hand, in linear wormlike micelles, although the normalized velocity profiles show a fore-and-aft symmetry at low Wi numbers, a strong negative wake and a stagnation point flow appear downstream of the falling sphere at higher Wi numbers. The stagnation point is located at $(X - a)/a \approx -3$ downstream of the falling sphere. This behavior is expected and has been reported in previous studies with linear wormlike micellar solutions[17, 19].

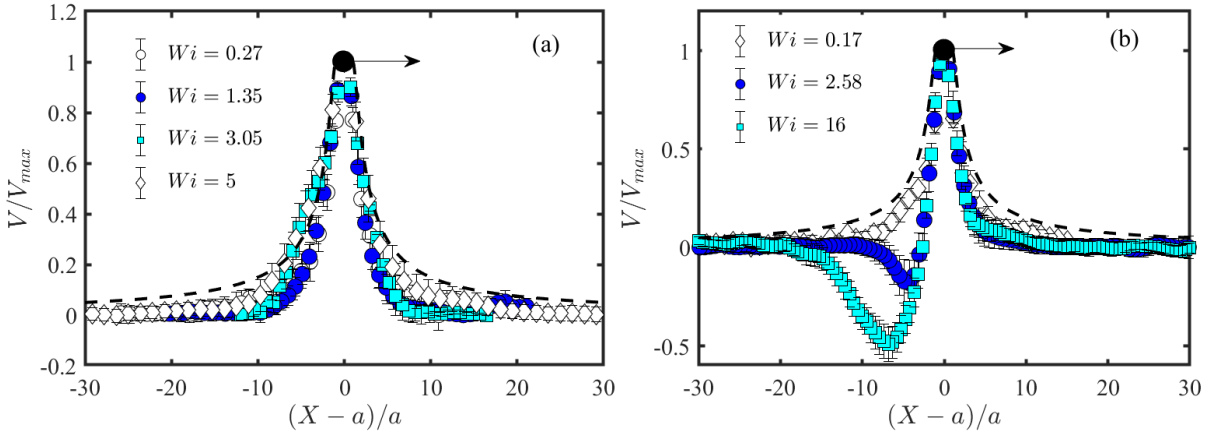

FIG. 3. Normalized fluid velocity as a function of distance along the axis of sphere center of mass for branched (a) and linear (b) wormlike micellar solutions. The sphere to tube size ratio $a/\Re = 0.037$ in branched micelles and $a/\Re = 0.056$ in linear wormlike micellar experiments. The dashed line represents the prediction of Stokes' analytical solution at vanishingly small Reynolds numbers.

The form of flow structure around a falling sphere in viscoelastic fluids has been extensively studied both experimentally and theoretically [45–48]. Through their large-scale numerical calculations, Harlen[47] and Bush [48] demonstrated that the flow structure downstream of the falling spheres is controlled by the competition between normal stress differences in uniaxial extensions and normal stress differences in simple shear flows. The ratio of these two forces can be expressed as Tr/Wi, where Trouton ratio (Tr) and Weissenberg numbers Wi represent strength of the extensional flow and the shear flow. Based on the theoretical analyses of Harlen and Bush, below a critical threshold of this dimensionless parameter, a negative wake forms in the rear of the falling sphere. Later, Arigo and McKinley illustrated that this critical threshold is also impacted by the sphere to fluid column size ratio $a/\Re$, and have slightly modified this criterion by including the size ratio as $C = Tr/Wi.(a/\Re)$. Therefore, it is expected that a negative wake appears downstream of a falling sphere in viscoelastic fluids for C values below a critical threshold.

To check whether the above criterion can rationalize the differences observed in the linear and branched micelles, we have plotted our experimental results in terms of the dimensionless number C (see Fig. 4). Note in calculating C we have used the maximum Trouton ratios of the two fluids Tr_∞ measured via the DoS technique. Empty and filled symbols represent cases with no stagnation point and stagnation point flow, respectively. For the linear wormlike micelles the negative wake appears below a critical threshold $C \approx 2$. However, for the branched micelles although experiments allow for much lower C values, the negative wake is not observed. This result clearly indicates that other parameters besides bulk shear, extensional rheology or sphere to tube size ratio play a key role in controlling the form of flow structure around the falling sphere in branched micelles.

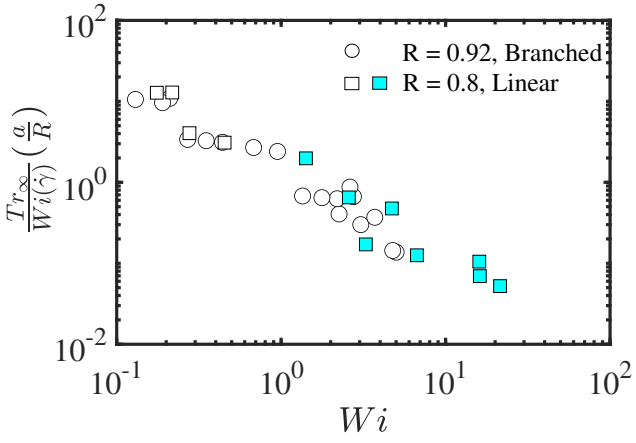

FIG. 4. Dimensionless $C = (Tr_\infty/Wi(\dot{\gamma})).(a/\Re)$ parameter as a function of Wi number for linear (squares) and branched (circles) micellar solutions. Empty symbols denote experiments with no negative wake, while filled symbols correspond to experiments for which the negative wake is observed.

D. Flow-Induced Birefringence

To further assess the effects of micellar structure on flow around the falling sphere, we performed full field flow-induced birefringence analysis. Flow-induced birefringence measurements enable us to access some flow features (micellar orientation and alignment) that are not detected by conventional methods such as PIV or PTV. Flow induced birefringence has been typically used in two-dimensional flows of wormlike micelles including flow past a stationary cylinder[49, 50] or cross-slot geometry[51–53]. Flow past a falling sphere is three-dimensional, which means that the micellar alignment and orientations are spatially averaged along the path of the light and therefore, the retardation and the extinction angles measured in this study are in fact spatially averaged values. Fig. 5 shows the averaged retardation and the extinction fields measured for the linear wormlike micellar solution around the falling sphere at a fixed sphere to tube size ratio $a/\Re = 0.056$, various Wi numbers, and vanishingly small Reynolds numbers. At small Weissenberg numbers $Wi = 0.2$, the time averaged birefringence intensity is uniformly small around the falling sphere. This is not surprising because at such small Wi numbers, micelles do not stretch, and therefore, fluid shows no signs of birefringence. Additionally, the measured average extinction angles vary between 0-45°, which suggests that micelles are randomly oriented in the flow direction. Note that the characteristic extinction angle for isotropic wormlike micellar fluids[54, 55] or polymer melts[56] is defined as 45° in the literature, which agrees with the maximum extinction angle measured in our experiments at low Wi numbers. Therefore, to be consistent with the literature, we use the numerical values of the maximum extinction angle at low Wi numbers (i.e., $\bar{\chi} \approx 45°$) to denote the random orientation of micelles around the falling sphere. As Wi number increases to $Wi = 2.6$, and therefore, the flow is strengthened, a small birefringent band forms downstream of the sphere center of mass. At still stronger flows with $Wi = 16$, the transmitted light intensity contrast sharpens, and the birefringence band grows markedly in the wake of the falling sphere. This birefringence band reflects the increased alignment of wormlike micelles along the extensional flow direction. Within this birefringent band, the micelles are fully aligned in the direction of flow with an extinction angle $\bar{\chi} \approx 0°$, which is consistent with previous measurements in extensional flows of polymer solutions[57], colloidal rods[58] and in flow of wormlike micelles past a falling sphere[16].

On the other hand, Fig. 6 shows flow-induced birefringence results for spheres with $a/\Re = 0.056$ at various Wi numbers in the branched micellar solution. Similar to linear wormlike micelles, the branched micelles do not show any significant birefringence up to $Wi = 0.44$, and the resulting averaged extinction angles vary as $\bar{\chi} \approx 0 - 45°$. At $Wi = 0.44$, branched micelles become weakly birefringent. However, at $Wi = 2.2$, branched micelles demonstrate a strong birefringent behavior and the extinction angle approaches $\bar{\chi} \approx 0°$ in the wake of the falling sphere. Further increase of the Wi number to $Wi = 3.7$ gives rise to a broader birefringence band downstream of the sphere center of mass with extinction angles $\bar{\chi} \approx 0°$ (see also Fig. S4 in the supplementary materials.). Beyond $Wi \approx 1$, birefringence intensity and the extinction angle inside the band become practically constant, reflecting quasi-saturation of alignment of the branched wormlike chains in the band. It is worth noting that at an approximately similar Wi numbers, not only the branched micelles exhibit a much stronger birefringent band, but also the birefringent band is much thicker in branched micellar solution than its linear counterpart (compare Fig. (6) with Fig. (5)).

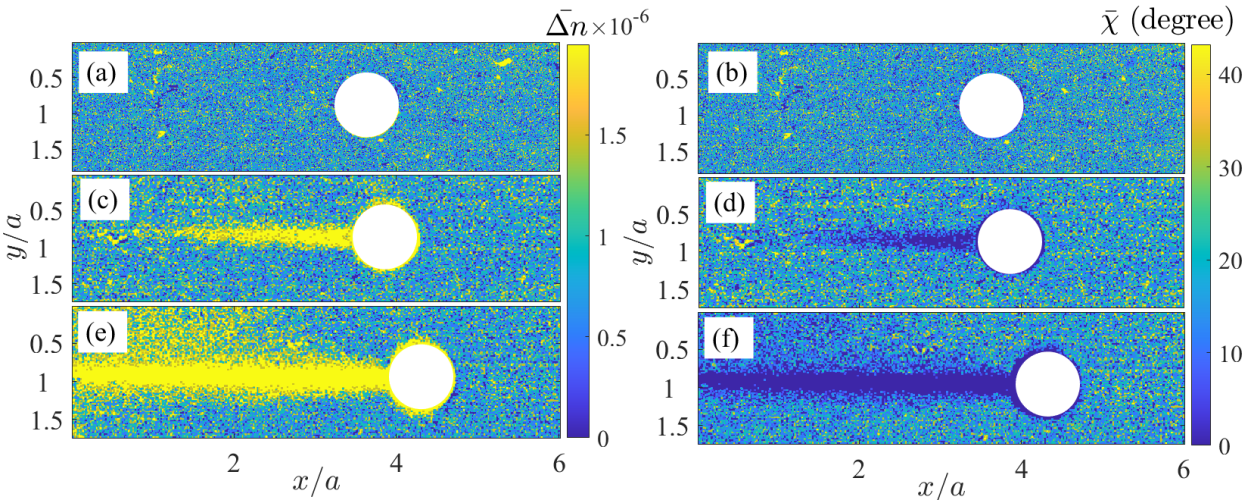

FIG. 5. Averaged birefringence intensity (false color) $\bar{\Delta n}$ around the falling sphere (left panel) and the averaged extinction angle $\bar{\chi}$ (right panel) calculated for the linear wormlike micellar solution. Experimental conditions are as follows: (a,b) $Wi = 0.2$ and $Re = 1.39 \times 10^{-5}$, (c,d) $Wi = 2.6$ and $Re = 3.37 \times 10^{-4}$ and (e,f) $Wi = 16$ and $Re = 1.7 \times 10^{-2}$. The sphere to fluid column size ratio in all of these experiments is fixed at $a/\Re = 0.056$.

Fig. 7 shows the averaged birefringence intensity of the linear and branched micelles at a distance equal to one sphere diameter away from the sphere center of mass downstream of the falling sphere. For both linear and branched micellar solutions, the micelles become more birefringent as the Wi number increases. The branched micelles are typically more birefringent than the linear micelles for $0.1 < Wi < 3$. Additionally, for both micellar solutions the birefringence intensity is saturated beyond a critical Weissenberg number ($Wi \approx 1$ for branched micelles and $Wi \approx 2.5$ for linear micelles).

Thus far, our experiments have indicated that the steady flow of branched micelles around the falling sphere is characterized by i) fore-and-aft symmetric velocity profiles, ii) an apparent local maximum in the drag correction factor and iii) a stronger birefringence than the linear micelles in an otherwise identical condition. But, how can branched micelles show a Newtonian-like flow profile in the wake of a falling sphere and at the same time impart a strong birefringence? The difference between the flow structure in linear and branched micelles could be linked to the micellar microsructure. Chellamuthu and Rothstein[28] investigated the uniaxial stretching of branched micelles in a filament stretching rheometer and showed that at high enough branching densities, the Trouton ratio asymptotes to 3, indicating that highly branched micelles exhibit Newtonian-like behavior in extensional flows. Chellamuthu and Rothstein linked this behavior to additional stress relaxation mechanism that is available to branched micelles through ghost-like crossing of the branched junctions. Their findings are consistent with our flow profile measurements that demonstrate a Newtonian-like flow and a near unity drag correction factor around the falling sphere in branched micelles. Unlike polymers, the branched points in micellar solutions are not fixed and can slide along the micelles chain backbone, giving rise to an additional stress relaxation mechanism. Our hypothesis is that at the range of Weissenberg numbers corresponding to steady flow behavior $1 < Wi < 5$, branched micelles can relax the stresses around the falling sphere much

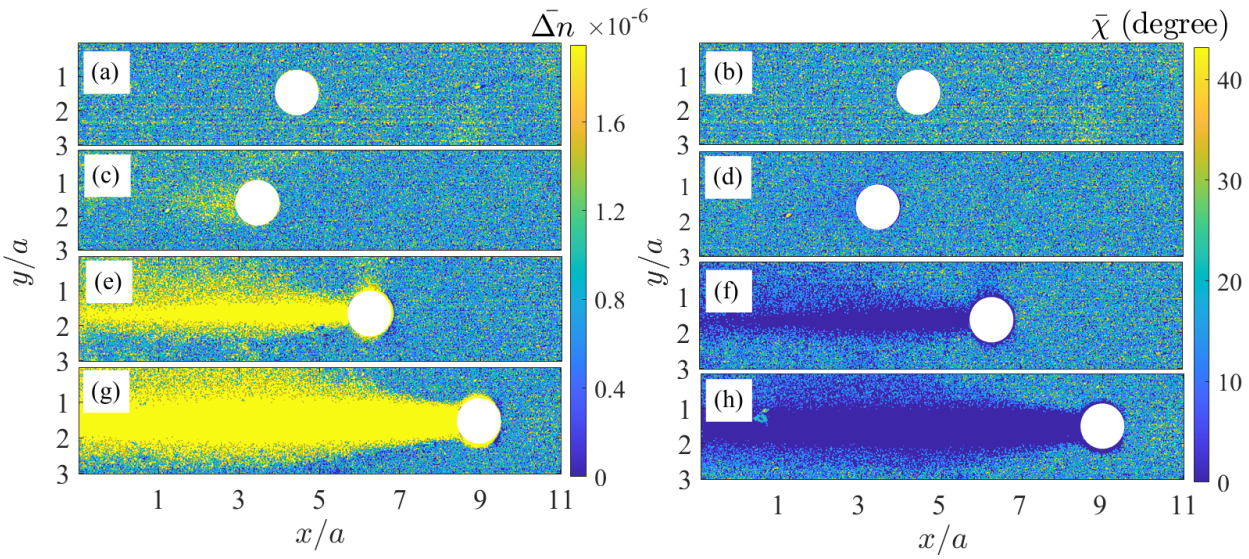

FIG. 6. Averaged birefringence intensity $\bar{\Delta n}$ (false color) around the falling sphere (left panel) and the averaged extinction angle $\bar{\chi}$ (right panel) calculated for the branched wormlike micellar solution. Experimental conditions are as follows: (a,b) $Wi = 0.13$ and $Re = 1.4 \times 10^{-5}$, (c,d) $Wi = 0.44$ and $Re = 6.8 \times 10^{-5}$, (e,f) $Wi = 2.2$ and $Re = 1.00 \times 10^{-3}$ and (g,h) $Wi = 3.7$ and $Re = 4.9 \times 10^{-3}$. The sphere to fluid column size ratio in all of these experiments is fixed at $a/\Re = 0.056$.

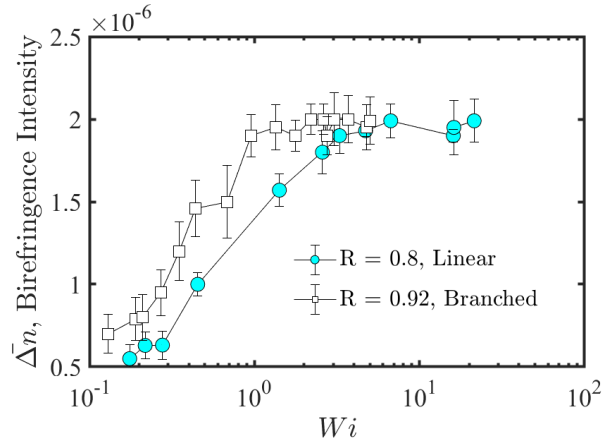

FIG. 7. Time averaged birefringence intensity $\bar{\Delta n}$ as a function of Wi number for linear (filled circles) and branched (empty squares) wormlike micellar solutions.

more efficiently than the linear wormlike micelles by ghost-like crossing. This additional stress relaxation mechanism not only gives rise to a Newtonian-like flow profile around the falling sphere and an almost Newtonian drag correction factor, but also may further facilitate alignment and orientation of the branched micelles around the falling sphere. Note that the upturn in the drag correction factor in branched micelles is not likely caused by micelles extensional hardening because linear wormlike micelles exhibit a stronger extensional hardening response than the branched wormlike micelles (see Fig. 1 (d)).

E. Unsteady Flow

As flow around the falling sphere is strengthened, both branched and linear micellar fluids experience a flow instability that is characterized by acceleration and deceleration in sphere sedimentation velocity. The sphere drag correction factor decays upon increasing the flow strength in unsteady flow regime. According to Chen and Rothstein, the instability in sphere sedimentation experiments is due to flow-induced micellar breakage en masse[16]. Therefore, the reduction in sphere drag correction factor in unsteady flow regime is caused by increasing possibility of the flow-induced micellar breakage at higher characteristic Wi numbers.

Fig. 8(a) shows the time-resolved velocity of the sphere center of mass for a sphere with $a/\Re = 0.037$ and various Wi and Wi_E in the linear and branched micellar solutions. It is worth noting that fluctuations in the sphere sedimentation velocity are random such that the dominant frequency of these fluctuations is rather very broad both in the linear and branched micellar solutions. Additionally, the flow field around a falling unsteady sphere is resolved in the linear and branched micellar solutions. Fig. 8(b,c) show the 2D time-resolved velocity vectors around the falling sphere during the acceleration-deceleration time window denoted in Fig. 8(a). Interestingly, the flow fields around the falling sphere at the moment of instability are qualitatively different for the linear and branched micellar fluids. In branched micellar solution, and following the onset of instability, a wave forms from in the wake of the falling sphere, and start propagating away from the falling sphere. This wave is likely elastic in nature because of the large elasticity $El = Wi/Re$ of the wormlike micellar solutions. For experiments with branched micelles fluid elasticity varies as $El \approx 90 - 9 \times 10^4$, and for linear micelles $El \approx 30 - 8 \times 10^4$. Evidently, this wave can propagate long enough distances all the way to the cylinder walls, forming four vortices around the falling sphere in branched micelles. Whereas, the linear micellar solution, although experiencing a stronger flow (higher Wi), does not show a strong enough elastic wave capable of generating obvious recirculation regions. To assess the effects of elastic wave on the flow structure around the falling sphere, a viscoelastic Mach number can be defined as: $Ma = V_{max}/\upsilon$, where velocity of the propagating wave $\upsilon = \sqrt{G_0/\rho_f}$. The viscoelastic Ma number quantifies the relative strength of the local flow velocity (V_{max}) to wave propagation velocity (υ). The two wormlike micellar solutions of this study are Maxwellian fluids, therefore, the plateau modulus can be estimated as $G_0 = \eta_0/\lambda$, which leads to $Ma = V_{max}/\upsilon = \sqrt{Wi.Re_0}$. Fig. 9 shows the viscoelastic Mach number as a function of Wi for sphere sedimentation experiments in the linear and branched micellar solutions. The resulting viscoelastic Mach numbers are typically larger in experiments with the branched micelles than the linear micelles. In particular, for unstable sphere sedimentation cases presented in Fig. 8, the viscoelastic Mach number in the branched micelles ($Ma \approx 0.22$) is larger than in the linear micelles ($Ma \approx 0.1$), which suggests that following the instability, the wave that form may propagate easier in branched micelles. Our hypothesis is that the branched micelles may form an intertwined connected network of micelles that help facilitate the propagation of elastic waves around the falling sphere compared to the linear micelles.

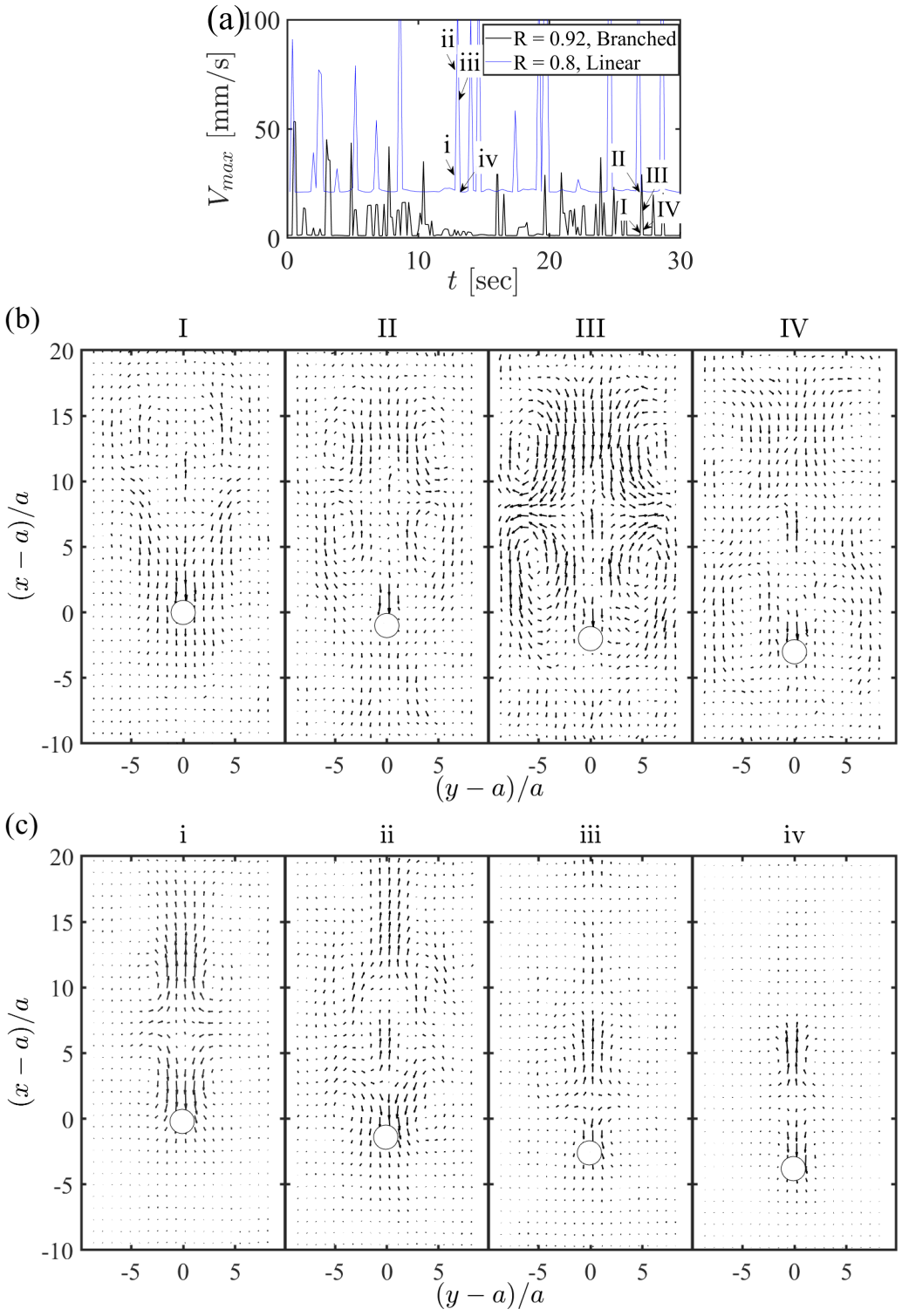

FIG. 8. (a) Time-resolved velocity of the sphere center of mass in linear and branched micelles. Note that the velocity data for linear micellar solution are shifted up for visual clarity. (b) The 2D velocity vectors around the falling sphere in the branched micellar solution at $Wi = 26.5$, $Wi_E = 26.5$, and $Re = 2 \times 10^{-2}$. (c) 2D velocity vectors around the falling sphere in linear wormlike micellar solution at $Wi = 54.5$, $Wi_E = 27.8$, and $Re = 5 \times 10^{-2}$. The sphere to fluid column size ratio is fixed at $a/\Re = 0.037$.

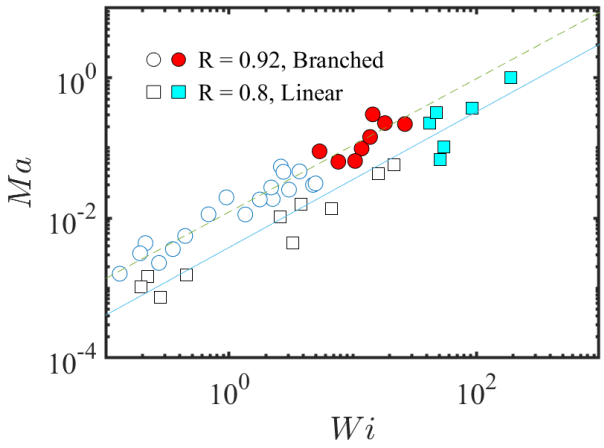

FIG. 9. Viscoelastic Mach number as a function of Weissenberg number for sphere sedimentation experiments in linear and branched micellar solutions. The empty and filled symbols denote the steady and unsteady sphere sedimentation cases, respectively. The dashed and continuous lines correspond to the best power-law fit of $Ma \propto Wi^{0.95}$ to the experimental data of branched and linear micellar solutions, respectively.

Mohammadigoushki and Muller[17] proposed a criterion based on the extensional Weissenberg number that successfully separated steady from unsteady sphere sedimentation regimes from each other. This criterion is independent of the surfactant chemistry and/or the shear banding behavior. To test the applicability of this criterion for branched micellar solutions, we have calculated both Wi and Wi_E in a similar fashion to our previous studies for unsteady flow experiments. Fig. 10(a) shows that resulting Wi numbers as a function of Re for experiments reported in this study along with the literature values. As expected, the criterion based on $Wi - Re$ is not capable of explaining the onset of instability in our experiments. On the other hand, Fig. 10(b) shows similar experimental results plotted based on $Wi_E - Re$. Clearly the steady and unsteady flow regimes are still separated. Despite some local differences in the flow field around the falling spheres in linear and branched micelles, the critical threshold for onset of instability is unaffected by the micellar microstructure.

IV. ACKNOWLEDGMENTS

HM is supported by US National Science Foundation through award CAREER CBET 1942150.

V. SUMMARY

We presented a detailed study on the flow of linear and branched micellar solutions past a falling sphere. The three key findings in steady flow regime can be summarized as follows:

1. A falling sphere experiences a near unity drag correction factor in both linear and branched micelles for $Wi < 1$. While at higher Wi numbers, a significant drag reduction is reported in linear wormlike micelles, an apparent maximum with drag correction

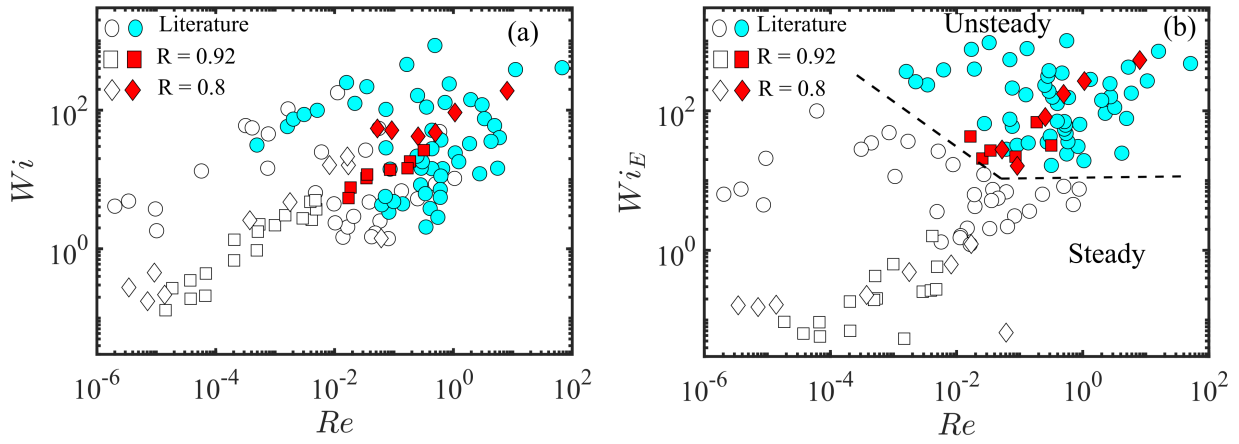

FIG. 10. The phase diagrams for sphere sedimentation experiments based on (a) $Wi - Re$ and (b) $Wi_E - Re$. The empty and filled symbols correspond to the steady and unsteady sphere sedimentation experiments. The literature data are extracted from[17, 23].

factors $K_{max} \approx 0.75$ is observed for branched micelles. The drag correction factors in branched micelles for $Wi > 1$ are always higher than the linear wormlike micelles.

2. Subject to weak flows (i.e., $Wi < 1$), the flow structure around the falling sphere is characterized by a fore-and-aft symmetry both in the linear and branched micelles. At higher Wi numbers, the linear wormlike micellar fluid exhibits a strong negative wake downstream of the falling sphere, while branched micelles still show a fore-and-aft symmetry. The criterion proposed by Arigo and McKinley ($C = Tr/Wi(\dot{\gamma}).a/\Re$) does not capture the different flow structures reported in the linear and branched micelles, indicating that micellar branching has contributed significantly to the form of flow structure around the falling sphere.

3. Flow induced-birefringence measurements around the falling sphere illustrated that the branched micelles are more birefringent than the linear wormlike chains in an otherwise identical condition.

Our hypothesis is that the additional stress relaxation mechanism via ghost-like crossing of branched points is highly effective such that not only it leads to a Newtonian flow structure and an upturn in sphere drag correction factor, but also may facilitate micellar orientation, and hence, gives rise to a stronger flow-induced birefringence around the falling sphere.

In addition to the steady flow regime, we have reported unsteady sphere sedimentation behavior both in the linear and branched micellar solutions. The resulting sphere drag correction factor always decreases upon increasing Wi number presumably due to flow-induced micellar breakage. Despite some differences in detailed form of the flow structure around the falling sphere in linear and branched micelles, our results corroborate the previously proposed criterion based on $Wi_E - Re$ for the onset of instability. Therefore, we can conclude that micellar branching does not affect the mechanism of instability.

Finally, the results of this study reveal the importance of micellar branching on flow around a falling sphere where a combination of shear and extensional flow is present. The correspondence (or the feedback loop) between the flow field and micellar topology may also impact dynamics of wormlike micelles in simple shear flows (e.g., Lutz-Bueno et al.[59]) or other types of complex flows (e.g., contraction-expansion, cross-slot, flow past a cylinder and etc.). Additionally, currently available theoretical models on flows of wormlike micelles have not included the effects of micellar branching. Hence, this study opens a new direction with tantalizing opportunities for future experimental and theoretical studies of wormlike micelles.

1 T. Imae, R. Kamiya and S. Ikeda, *J. Colloid Interf. Sci.*, 1985, **108**, 215–225.
2 J. N. Israelachvili, *Intermolecular and Surface Forces*, Academic press, 2015.
3 H. Rehage and H. Hoffmann, *Mol. Phys.*, 1991, **74**, 933–973.
4 V. Croce, T. Cosgrove, G. Maitland, T. Hughes and G. Karlsson, *Langmuir*, 2003, **19**, 8536–8541.
5 S. R. Raghavan, G. Fritz and E. W. Kaler, *Langmuir*, 2002, **18**, 3797–3803.
6 V. Croce, T. Cosgrove, C. A. Dreiss, S. King, G. Maitland and T. Hughes, *Langmuir*, 2005, **21**, 6762–6768.
7 L. Ziserman, L. Abezgauz, O. Ramon, S. R. Raghavan and D. Danino, *Langmuir*, 2009, **25**, 10483–10489.
8 Z. Lin, *Langmuir*, 1996, **12**, 1729–1737.
9 C. Oelschlaeger, M. Schopferer, F. Scheffold and N. Willenbacher, *Langmuir*, 2009, **25**, 716–723.
10 G. Porte, R. Gomati, O. El Haitamy, J. Appell and J. Marignan, *J Phys Chem*, 1986, **90**, 5746–5751.
11 C. A. Dreiss, *Soft Matter*, 2007, **3**, 956–970.
12 J. Yang, *Current Op. in Colloid and Interf. sci.*, 2002, **7**, 276–281.
13 J. Myska and J. L. Zakin, *Ind. and Eng. Chem. Research*, 1997, **36**, 5483–5487.
14 J. L. Zakin, J. Myska and Z. Chara, *AlChE J.*, 1996, **42**, 3544–3546.
15 A. Jayaraman and A. Belmonte, *Phys. Rev. E*, 2003, **67**, 065301.
16 S. Chen and J. P. Rothstein, *J. Non-Newtonian Fluid Mech.*, 2004, **116**, 205–234.
17 H. Mohammadigoushki and S. J. Muller, *J. Rheol.*, 2016, **60**, 587–601.
18 N. Kumar, S. Majumdar, A. Sood, R. Govindarajan, S. Ramaswamy and A. Sood, *Soft Matter*, 2012, **8**, 4310–4313.
19 H. Mohammadigoushki and S. J. Muller, *J. Non-Newtonian Fluid Mech.*, 2018, **257**, 44–49.
20 M. Cates and S. Candau, *J. Phys. Condens. Matter*, 1990, **2**, 6869.
21 J. P. Rothstein, *J. Rheol.*, 2003, **47**, 1227–1247.
22 S. Wu and H. Mohammadigoushki, *J. Rheol.*, 2018, **62**, 1061–1069.
23 Y. Zhang and S. J. Muller, *Phys. Rev. Fluids*, 2018, **3**, 043301.
24 S. Wu and H. Mohammadigoushki, *Phys. Rev. Fluids*, 2019, **4**, 073303.
25 C. Sasmal, *J. Fluid Mech.*, 2021, **912**, A52.
26 J. P. Rothstein and H. Mohammadigoushki, *J. Non-Newtonian Fluid Mech.*, 2020, **285**, 104382.
27 Y. Zhang, H. Mohammadigoushki, M. Y. Hwang and S. J. Muller, *Phys. Rev. Fluids*, 2018, **3**, 093301.

28 M. Chellamuthu and J. P. Rothstein, *J. Rheol.*, 2008, **52**, 865–884.
29 R. Omidvar, S. Wu and H. Mohammadigoushki, *J. Rheol.*, 2019, **63**, 33–44.
30 D. Sachsenheimer, C. Oelschlaeger, S. Müller, J. Küstner, S. Bindgen and N. Willenbacher, *J. Rheol.*, 2014, **58**, 2017–2042.
31 L. M. Gouveia and A. J. Muller, *Rheol. Acta*, 2009, **48**, 163–175.
32 P. Rassolov and H. Mohammadigoushki, *J. Rheol.*, 2020, **64**, 1161–1177.
33 V. Aswal, P. Goyal and P. Thiyagarajan, *The Journal of Physical Chemistry B*, 1998, **102**, 2469–2473.
34 H. Rehage and H. Hoffmann, *J Phys Chem*, 1988, **92**, 4712–4719.
35 F. Lequeux, *Europhys. Lett.*, 1992, **19**, 675–681.
36 J. Dinic and V. Sharma, *Proc. Natl. Acad. Sci.*, 2019, **116**, 8766–8774.
37 J. Dinic, Y. Zhang, L. N. Jimenez and V. Sharma, *ACS Macro Lett.*, 2015, **4**, 804–808.
38 S. Wu and H. Mohammadigoushki, *Phys. Rev. Fluids*, 2020, **5**, 053303.
39 H. Ewers, A. E. Smith, I. F. Sbalzarini, H. Lilie, P. Koumoutsakos and A. Helenius, *Proc. Natl. Acad. Sci.*, 2005, **102**, 15110–15115.
40 W. Thielicke and E. Stamhuis, *Journal of Open Research Software*, 2014, **2**, year.
41 G. G. Fuller, *Optical rheometry of complex fluids*, Oxford University Press on Demand, 1995.
42 D. Gaudino, R. Pasquino and N. Grizzuti, *J. Rheol.*, 2015, **59**, 1363–1375.
43 G. C. S. Holder, W. Samuel. and H. Mohammadigoushki, *Accepted in Langmuir*, 2021.
44 B. Mena, O. Manero and L. Leal, *J. Non-Newtonian Fluid Mech.*, 1987, **26**, 247–275.
45 D. Fabris, S. J. Muller and D. Liepmann, *Phys. Fluids*, 1999, **11**, 3599–3612.
46 M. T. Arigo and G. H. McKinley, *Rheol. Acta*, 1998, **37**, 307–327.
47 O. G. Harlen, *J. Non-Newtonian Fluid Mech.*, 2002, **108**, 411–430.
48 M. Bush, *J. Non-Newtonian Fluid Mech.*, 1994, **55**, 229–247.
49 Y. Zhao, A. Q. Shen and S. J. Haward, *Soft Matter*, 2016, **12**, 8666–8681.
50 G. R. Moss and J. P. Rothstein, *J. Non-Newtonian Fluid Mech.*, 2010, **165**, 1505–1515.
51 J. A. Pathak and S. D. Hudson, *Macromolecules*, 2006, **39**, 8782–8792.
52 N. Dubash, P. Cheung and A. Q. Shen, *Soft Matter*, 2012, **8**, 5847–5856.
53 S. J. Haward, T. J. Ober, M. S. Oliveira, M. A. Alves and G. H. McKinley, *Soft Matter*, 2012, **8**, 536–555.
54 J.-F. Berret, in *Rheology of Wormlike Micelles: Equilibrium Properties and Shear Banding Transitions*, ed. R. G. Weiss and P. Terech, Springer Netherlands, Dordrecht, 2006, pp. 667–720.
55 S. Lerouge, J.-P. Decruppe and P. Olmsted, *Langmuir*, 2004, **20**, 11355–11365.
56 C. C. Hua, J. D. Schieber and D. Venerus, *J. Rheol.*, 1999, **43**, 701–717.
57 S. J. Haward, G. H. McKinley and A. Q. Shen, *Sci. Rep.*, 2016, **6**, 33029.
58 V. Calabrese, S. J. Haward and A. Q. Shen, *Macromolecules*, 2021.
59 V. Lutz-Bueno, R. Pasquino, S. J. Haward, A. Q. Shen and P. Fischer, *J. Rheol.*, 2017, **61**, 769–783.